Characterization of a broad-energy Germanium spectrometer

Author: Queralt Martín Saladich
Facultat de Física, Universitat de Barcelona, Diagonal 645, 08028 Barcelona, Catalonia, Spain

Advisor: José M. Fernández-Varea

Germanium detectors are widely used in γ-ray spectrometry. In this TFG we have performed the energy, resolution and efficiency calibrations of a broad-energy Ge spectrometer using a set of radioactive sources. The efficiency was also studied with Monte Carlo simulations. Furthermore, the properties of characteristic x-rays, annihilation and escape peaks were analysed. Modelling proved the excellent linearity and resolution of the detector, while the experimental efficiency differed somewhat from the simulation results. Parameter findings were in strong agreement with the literature data and Doppler broadening was confirmed for the annihilation peaks.

I. INTRODUCTION

The spectrometry of γ-rays and x-rays plays an important role in nuclear and atomic physics. It is also essential in many materials science techniques as well as in medical physics applications like radiology and radiotherapy. Broad-energy hyperpure Germanium (BEGe) detectors allow to work in a wide range of energies while having an excellent energy resolution [1, 2]. The principle of operation of these devices starts with the energy deposited by the impinging photons in the sensitive volume. The possible interaction mechanisms are photoelectric absorption, Compton scattering and electron-positron pair production, the latter only possible above $2m_ec^2$ [1, 3, 4]. The sensitive material (Ge) is connected to a bias voltage so that the electron-hole pairs produced by the electrons (or positrons) ejected in the fully-depleted semiconductor are pulled to the electrodes, generating an electrical signal. The height (voltage) of each collected pulse is proportional to the energy deposited in the sensitive material by the incident photon. In particular, if the photon deposits all its energy into the detector the spectrum will display a peak named full-energy (FE) peak.

The aim of this TFG was to calibrate a BEGe spectrometer using the FE peaks in the spectra of various radionuclides, and to analyse its energy resolution and efficiency. The efficiency was also studied with the DETEFF software [5]. Besides, a detailed investigation of the properties of other γ-rays and x-rays was performed, including the Doppler broadening of annihilation radiation [6], the intensity of characteristic x-rays and the presence of Ge K escape peaks. The original plan included the analysis of a natural radioactive source of ^{232}Th present in a sample of sand from the Guarapari beach (Brazil), but due to the COVID-19 pandemic the data could not be collected.

II. SPECTRA ACQUISITION

Data acquisition was carried out at the Servei d'Anàlisi Isotòpica (Facultat de Química) using a cylindrical BEGe detector coupled to a multi-channel analyser (4096 channels) under the guidance of Dr. Joana Tent. The equipment consisted of a CANBERRA BE3830 spectrometer, whose specifications are shown in Table I, a preamplifier (2002CPSL) [7] and a cryostat (7500SL). The refrigeration with liquid N_2 avoided thermal promotions that would otherwise happen owing to the small energy gap of Ge [2]. The detector window was made of carbon epoxy, a material that provides excellent transmission even at very low energies. In fact, the BE3830 detector covers the energy range from 3 keV to 3 MeV with high resolution for both low- and high-energy photons [8]. The detector is surrounded by a thick Pb shielding to minimize unwanted background (bg) radiation.

Table I: Specifications of the BE3830 detector and experimental conditions.

Parameter	Value
Active volume diameter	69.56 mm
Active volume thickness	30 mm
Window thickness	0.5 mm
Distance from window	5 mm
Source-detector distance	(87 ± 1) mm

5 certified point-like radioactive sources were employed in the analysis, namely ^{137}Cs, ^{60}Co, ^{22}Na, ^{241}Am and ^{133}Ba. The sources were positioned on the symmetry axis of the spectrometer at a fixed distance. The acquisition times were selected according to the activity of each source and its decay constant so as to assure enough counting statistics. Both the real and live times were recorded.

The collected raw spectra consist of the number of counted pulses associated to the channel n where they had been detected. The corresponding net spectra were obtained subtracting the rescaled background (bg) spectrum,

$$y_n^{\mathrm{net}} = y_n^{\mathrm{raw}} - \left(t_{\mathrm{live}}^{\mathrm{raw}}/t_{\mathrm{live}}^{\mathrm{bg}}\right) y_n^{\mathrm{bg}}, \qquad n \in [1, 4096], \quad (1)$$

where $t_{\mathrm{live}}^{\mathrm{raw}}$ and $t_{\mathrm{live}}^{\mathrm{bg}}$ are the live times. An example is shown in Fig. 1.

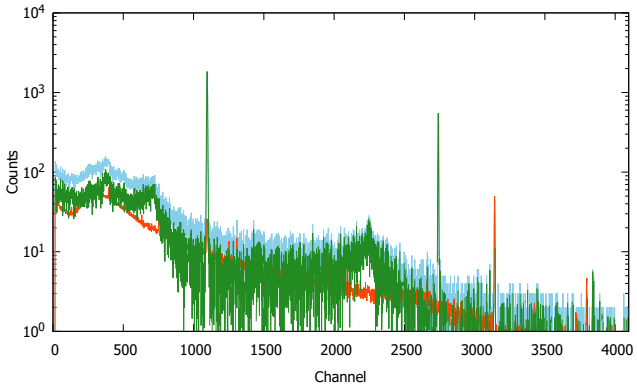

Figure 1: Raw (blue) and net (green) spectra of ^{22}Na. The rescaled bg spectrum (red) is also depicted.

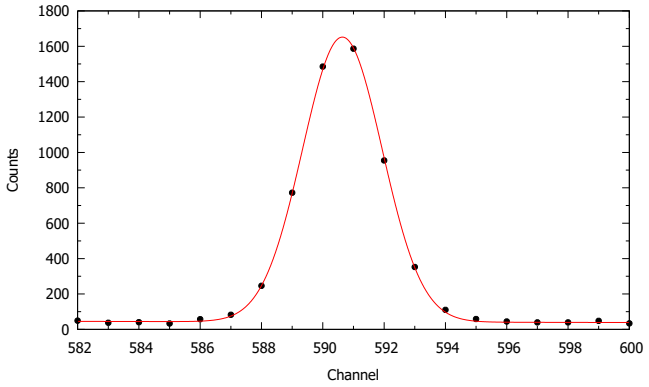

Figure 2: ROI in the spectrum of ^{133}Ba pertaining to the 276.4 keV γ-ray. The circles are the experimental data and the curve is the fitted model.

III. RESULTS AND DISCUSSION

A. Energy-channel relation

The energy calibration procedure began with the identification of 8 intense, isolated γ-ray peaks and their modelling adopting a Gaussian for the peak shape and a linear function for the continuous component of the spectrum,

$$\begin{aligned} G(n) &= N\,\frac{1}{\sqrt{2\pi\sigma^2}}\exp\left(-\frac{(n-\mu)^2}{2\sigma^2}\right), \\ C(n) &= c_0 + c_1 n. \end{aligned} \tag{2}$$

The continuous component interpolation was immediate. But to obtain the parameters μ, σ and N that define the Gaussian, a merit function was determined and minimized to adjust a parabola to the peak,

$$Q(\alpha,\beta,\gamma) = \sum_{n\in\mathrm{ROI}} \Big\{ \ln\left[y_n^{\mathrm{net}} - C(n)\right] - (\alpha+\beta n+\gamma n^2)\Big\}^2, \tag{3}$$

where ROI is the region of interest around the peak and $\ln G(n) = \alpha + \beta n + \gamma n^2$. The relationship between the Gaussian parameters in the two representations is

$$\sigma = \frac{1}{\sqrt{-2\gamma}}, \quad \mu = -\frac{\beta}{2\gamma}, \quad N = \sqrt{\frac{\pi}{-\gamma}}\exp\left(\alpha - \frac{\beta^2}{4\gamma}\right). \tag{4}$$

The minimization was done adopting the least-squares methodology with two different procedures to assure result consistency which included manual programming of the partial derivatives with respect to α, β and γ, equalling them zero and then solving the obtained 3×3 system using Python, and the fitting models available in Gnuplot which provided the uncertainties associated to the fitted parameters. Figure 2 displays the ROI of one of the γ-ray peaks of ^{133}Ba together with the fit.

Energy calibration consists in finding the parameters that suit the model $E(n) = a_0 + a_1 n$. The same procedure of minimization was applied using the merit function

$$Q(a_0,a_1) = \sum_j \left[E_j - (a_0 + a_1\mu_j)\right]^2, \tag{5}$$

being μ_j the centroid of the Gaussian that fits the j-th peak, whose energy E_j is extracted from the `nucleide` database [9]. The linear energy-channel relation showed an impressive Pearson correlation coefficient of $r = 0.999\,999\,998$, and the fitted parameters were $a_0 = 2.18(3)$ keV (offset) and $a_1 = 0.464\,304(13)$ keV/channel (gain). The experimental values and first-order fit are represented in Fig. 3.

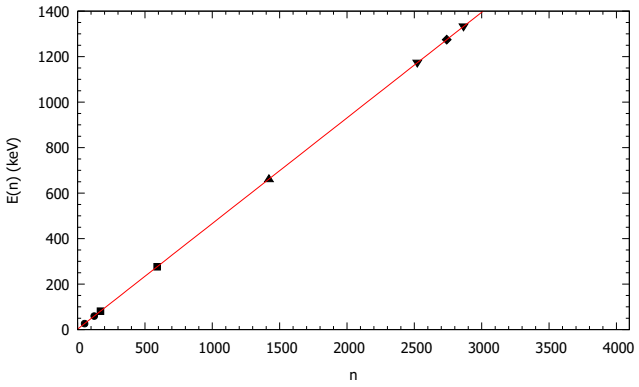

Figure 3: Energy calibration. Symbols are experimental data for each radionuclide and the straight line corresponds to the linear fit.

B. Energy resolution

The peaks in the spectra have a finite width due to statistical fluctuations in the number of produced electron-hole pairs (Gaussian) and the natural width of the electromagnetic transitions (Lorentzian), the former being

predominant. The variance of the Gaussian broadening is the sum of the following contributions [1]. **i)** Statistical fluctuations in the number of produced electron-hole pairs, $\sigma_{\rm st}^2 \propto E$. **ii)** Incomplete charge collection; however, $\sigma_{\rm cc} \approx 0$ because the detector is not thick enough for charge-carrier trapping effects to be relevant. **iii)** The variance $\sigma_{\rm el}^2$ of the electronic noise introduced by the amplification chain. The final energy-dependent standard deviation is the combination in quadrature

$$\sigma(E) = \sqrt{b_0 + b_1 E}. \tag{6}$$

The same minimization process as in the previous subsection was followed but now with the merit function

$$Q(b_0, b_1) = \sum_j \left[\sigma^2(E_j) - (b_0 + b_1 E_j)\right]^2. \tag{7}$$

The fit delivered $b_0 = 0.259(13)$ keV^2 and $b_1 = 4.46(17)\times 10^{-4}$ keV with a Pearson correlation coefficient $r = 0.996$. Other fitting functions have been proposed. For instance, CANBERRA's Genie 2000 Basic Spectroscopy Software implements the empirical relation $\sigma(E) = p_0 + p_1\sqrt{E}$ [10, 11]. Adjusting this model to the data yields $p_0 = 0.43(2)$ keV and $p_1 = 0.0131(8)$ keV$^{1/2}$ with $r = 0.984$.

Instead of σ it is customary to use the full width at half maximum FWHM $= 2\sqrt{2\ln 2}\,\sigma$ to quantify the energy resolution. The FWHM of the BEGe spectrometer is shown in Fig. 4 along with the two considered resolution functions. The FWHM measured by the manufacturer when the detector was purchased nearly 20 years ago are smaller. This worsening of the resolution is partly due to the ageing of the detector.

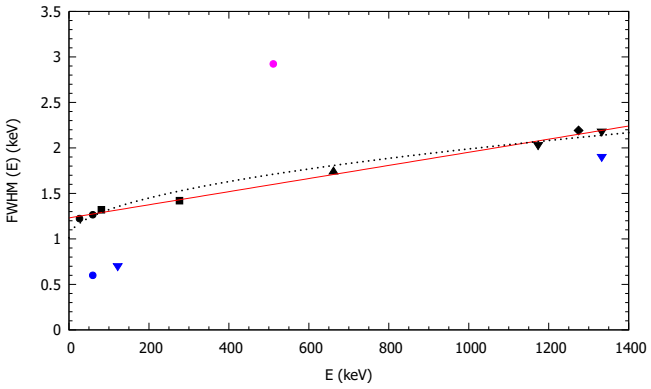

Figure 4: FWHM vs photon energy. Experimental data (black), detector specification values (blue) and Doppler-broadened annihilation peak of ^{22}Na (magenta). Eq. (6) and the empirical model adopted by Genie are shown as continuous and dashed curves, respectively.

C. Efficiency

The FE peak efficiency, $\varepsilon_{\rm FE}$, is defined as the probability that a photon emitted isotropically from the source enters the detector's active volume, interacts there, and the ensuing energy deposition gives rise to a count in the FE peak of the spectrum. The theoretical expression is

$$\varepsilon_{\rm FE}(E) = (\Omega/4\pi)\, T(E)\, \varepsilon(E), \tag{8}$$

where $\Omega/4\pi$ is the fraction of solid angle subtended by the detector (related to the source-detector distance and the detector diameter), $T(E) = \mathrm{e}^{-\mu_{\rm w}(E)\ell_{\rm w}}$ the transmission through the window ($\ell_{\rm w}$ is the thickness of the carbon epoxy window and $\mu(E)$ is the linear attenuation coefficient of this material), and $\varepsilon(E)$ the intrinsic efficiency, which is a complicated function of the detector geometry.

The experimental FE peak efficiency can be determined as

$$\varepsilon_{\rm FE}^{\rm exp}(E_j) = \frac{N_j}{\mathcal{A}_j I_j t_{{\rm real},j}}, \tag{9}$$

where N_j is the net area of peak j, $\mathcal{A}_j$ is the activity of the radioactive source, I_j is the yield (average number of photons emitted per decay), and $t_{{\rm real},j}$ is the real acquisition time. The activity is calculated from the initial activity, the decay constant [9], and the time elapsed between the certification date (March 1, 1997) and the experiment (February 17, 2020) by means of the well-known expression $\mathcal{A}_j = \mathcal{A}_{0,j}\,\mathrm{e}^{-\lambda_j \Delta t}$.

The FE peak efficiency curve was also evaluated using the DETEFF software, a simple user-friendly Monte Carlo code [12]. The program needs as input the geometry of the source/detector configuration as well as the energy of the emitted photons and the number of histories to be simulated. The precision of DETEFF was checked comparing its predictions to the values tabulated in Ref. [13] for a similar BEGe spectrometer and setup. Advisor J.M. Fernández-Varea computed the $\varepsilon_{\rm FE}(E)$ curve using the PENELOPE/penEasy program to reassure the consistency of the obtained results.

The $\varepsilon_{\rm FE}^{\rm exp}(E_j)$ values are systematically some 10% below the Monte Carlo curve for low-energy peaks. The observed discrepancy may be related to one or more causes [14]. **i)** The effect of the carbon epoxy window was evaluated doing simulations with and without this layer but no consequence on the results was found ($T(E) \approx 1$ above 10 keV [8]). **ii)** True coincidence summing reduces the counts in the FE peaks, especially when the source-detector distance is small (as in the present setup) and the source emits low-energy γ-rays and x-rays, e.g. ^{133}Ba and ^{241}Am [15]. **iii)** The thickness of the Ge sensitive medium might differ up to 1.5 mm from the nominal value [16, 17]. **iv)** The measured source-detector distance had an uncertainty of 1 mm, yielding a relative uncertainty of 2.3% in the efficiency. **v)** The presence of a thick Ge front dead layer, to be expected in aged detectors, would reduce the efficiency at low energies [18]. Addressing items **ii-v** is well beyond the present possibilities. It would require a better geometrical arrangement, additional radioactive sources and a multichannel analiser with more than 4096 channels.

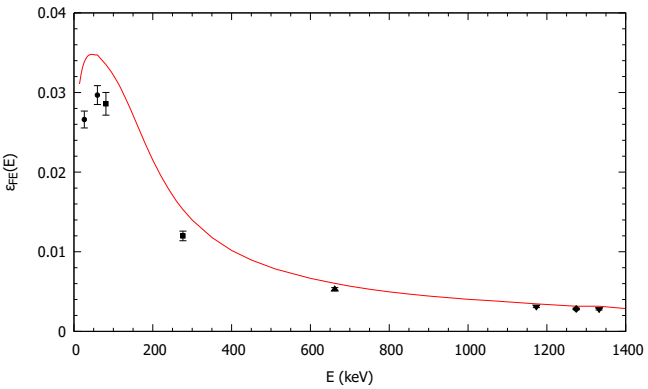

Figure 5: FE peak efficiency vs photon energy. The symbols are experimental data and the curve is the prediction of DETEFF. Uncertainties are one standard deviation.

D. Further peak analysis

Further analysis focused on the identification of other γ-rays, the FWHM of annihilation peaks, the intensity ratios of characteristic x-rays, and the presence of Ge K escape peaks. The energies of these additional peaks were computed using the linear energy-channel relation and compared to reference values [9, 19], see Table II.

Table II: Experimental and reference energies [9, 19] of the extra γ-rays, annihilation peaks, characteristic x-rays and Ge K escape peaks.

Nuclide	E_{exp} (keV)	E_{ref} (keV)	Type
^{133}Ba	53.21(5)	53.162	γ
bg ^{40}K	1460.60(8)	1460.822	γ
^{22}Na	510.91(5)	510.999	annihilation
bg	510.70(8)	510.999	annihilation
^{133}Ba	30.86(3)	30.973	$_{55}$Cs Kα
^{133}Ba	35.12(5)	34.987	$_{55}$Cs Kβ
^{137}Cs	32.06(4)	32.193	$_{56}$Ba Kα
^{137}Cs	36.53(8)	36.378	$_{56}$Ba Kβ
^{241}Am	13.91(4)	13.944	$_{93}$Np Lα
^{133}Ba	20.92(5)	21.087	Ge K escape
^{137}Cs	22.14(11)	22.307	Ge K escape

1) γ-rays were identified in the decay of ^{133}Ba and assigned to the initial and final nuclear levels of the daughter nucleus. The bg spectrum displayed a prominent peak due to ^{40}K, confirming the presence of this radionuclide in the environment, along with the peaks of radioactive nuclei belonging to the uranium series.

2) The FWHM of the 511 keV peak in the spectrum of ^{22}Na, 2.923 keV, is much larger than that predicted by the resolution curve, see Fig. 4. The broadening is caused by the motion of the electrons in the encapsulation of the source before they annihilate with the slowed-down positron created by the β^+ disintegration of ^{22}Na [10]. Choosing the positive z axis pointing from the source towards the detector, energy and linear momentum conservation for a stationary positron implies that the energy of the *detected* photon is $m_e c^2 - \frac{1}{2}U_i + \frac{c}{2}p_z$, where p_z is the z component of the linear momentum of the electron immediately before annihilating and U_i the binding energy of the electron's atomic (sub)shell. The photon energy experiences a fixed shift downwards plus a variable shift that depends on whether the electron was approaching to or receding from the detector just before annihilation. Taking into account the isotropic velocity distribution of the electrons we have $\langle p_z \rangle = 0$. However, $\langle p_z^2 \rangle \neq 0$, which adds a contribution $\sigma_D^2 = (c/2)^2 \langle p_z^2 \rangle$ to the variance, and therefore to the FWHM. The corresponding average kinetic energy of the electron is $\langle T \rangle = 3\langle p_z^2 \rangle / 2m_e \approx 12$ eV. An even larger Doppler broadening (FWHM = 3.257 keV) was found for the annihilation peak in the bg spectrum, indicating a broader velocity distribution of the electrons in the atoms located near the bg radionuclides that decay by β^+ disintegration. Moreover, $\langle T \rangle \approx 17$ eV. Since the ^{22}Na positrons annihilate in a low-Z surrounding (the source encapsulation is made of H, C and O), the shift and broadening are smaller than the corresponding values of the annihilation peak in the bg spectrum.

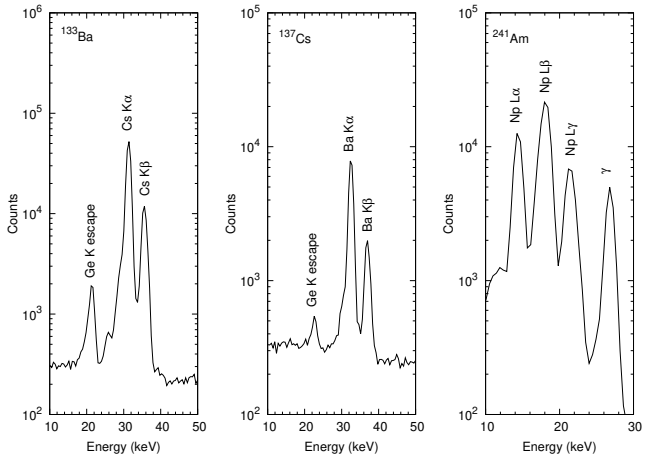

Figure 6: Characteristic K and L x-rays, and Ge K escape peaks for (a) ^{133}Ba, (b) ^{137}Cs and (c) ^{241}Am.

3) The nuclear processes of electron capture and internal conversion produce vacancies in the inner (sub)shells of the daughter atom, often in the K shell. This happens in the case of ^{133}Ba and ^{137}Cs, whose spectra (Figs. 6a and 6b) display Kα (KL$_{2,3}$) and Kβ (KM$_{2,3}$) characteristic x-rays that are emitted in the subsequent atomic relaxation. These doublets were fitted with Gaussian functions to get their net peak areas. The corresponding ratios, corrected for the *relative* efficiency, were compared to the theoretical ratios of Ref. [20]. The ratios are $[\text{K}\beta/\text{K}\alpha]_{\text{exp}} = 0.234(7)$ and $[\text{K}\beta/\text{K}\alpha]_{\text{th}} = 0.2240$ for $_{55}$Cs and $[\text{K}\beta/\text{K}\alpha]_{\text{exp}} = 0.226(7)$ and $[\text{K}\beta/\text{K}\alpha]_{\text{th}} = 0.2273$ for $_{56}$Ba. Similarly, in the spectrum of ^{241}Am (Fig. 6c)

we observed the Np Lα ($L_3M_{4,5}$) doublet as well as the Np Lβ and Lγ multiplets. The severe peak overlapping of lines in the multiplets precluded a detailed analysis.

4) Low-energy γ-rays undergo photoelectric absorption by the K-shell of Ge close to the frontal surface of the detector [2]. Ge Kα and Kβ x-rays can then be emitted, which have a non-zero probability to escape from the detector and produce escape peaks displaced to the left by $E_{\mathrm{Ge\,K}\alpha} = 9.886$ keV and $E_{\mathrm{Ge\,K}\beta} = 10.982$ keV. The presence of these peaks was corroborated in the spectra of ^{133}Ba and ^{137}Cs, Figs. 6a and 6b. The probability of Ge Kβ emission is smaller than that of Ge Kα, this explains the asymmetry of the escape peaks.

IV. CONCLUSIONS

The energy calibration confirmed the linearity of the BEGe spectrometer. The resolution analysis yielded parameters that matched those proposed in the literature and FWHM values displayed small peak widths meaning the detector was able to successfully resolve energy peaks with well-defined slim bell-shaped curves. Experimental efficiency values exhibited discrepancies with DETEFF simulations for low-energy peaks due to coincidence-summing phenomena. γ-ray energies were in good agreement with reference values. Doppler broadening was quantified in the annihilation peaks, showing wider FWHM values than expected. The x-ray modelling was consistent with atomic data tabulations when comparing K-shell peak areas. Ge K escape peaks were found for ^{133}Ba and ^{137}Cs and their energies matched the literature data.

The ability of BEGe spectrometers to perform accurate measurements is the reason for their successful use in many research areas. For instance, the excellent energy resolution makes them suitable to solve some limitations encountered in SPECT/CT medical imaging. And they are employed in proton-beam radiotherapy to measure secondary γ radiation emitted from the patient so as to provide precise *in vivo* information on the dose delivery.

Acknowledgments

I am grateful to my advisor José M. Fernández-Varea, for his invaluable guidance and helpful advice which have been essential for the development of this project. I would also like to thank Joana Tent, for her assistance with the experimental data acquisition; to my parents and my brother, for always encouraging me; and to Laia and Lídia, for being my unconditional support.

[1] Tsoulfanidis, N. & Landsberger, S. *Measurement and Detection of Radiation* (CRC Press, 2015), 4th edn.

[2] Devanathan, R., Corrales, L. R., Gao, F. & Weber, W. J. Signal variance in gamma-ray detectors—A review. *Nuclear Instruments and Methods A* **565**, 637–649 (2006).

[3] Gao, F. *et al.* Gamma-ray interaction in Ge: A Monte Carlo simulation. *Nuclear Instruments and Methods B* **255**, 286–290 (2007).

[4] Knoll, G. F. *Radiation Detection and Measurement* (John Wiley & Sons, 2010), 4th edn.

[5] Cornejo Díaz, N. & Jurado Vargas, M. DETEFF: An improved Monte Carlo computer program for evaluating the efficiency in coaxial gamma-ray detectors. *Nuclear Instruments and Methods A* **586**, 204–210 (2008).

[6] Coldwell, R. L. & Lasche, G. P. Experimental measurements of Doppler broadening of escape peaks in HPGe detectors. *Journal of Radioanalytical and Nuclear Chemistry* **307**, 2509–2512 (2016).

[7] CANBERRA. *Detector specification and performance data* (1999).

[8] MIRION. *Broad Energy Germanium Detectors* (2016).

[9] Bé, M.-M. *et al.* Table de Radionucléides. URL `http://www.nucleide.org`.

[10] Gilmore, G. R. *Practical Gamma-Ray Spectrometry* (John Wiley & Sons, 2008), 2nd edn.

[11] MIRION. *Genie 2000 Basic Spectroscopy Software* (2016).

[12] Carrazana González, J., Cornejo Díaz, N. & Jurado Vargas, M. Application of the Monte Carlo code DETEFF to efficiency calibrations for in situ gamma-ray spectrometry. *Applied Radiation and Isotopes* **70**, 868–871 (2012).

[13] Kramer, G. H., Crowley, P. & Burns, L. C. Investigating the impossible: Monte Carlo simulations. *Radiation Protection Dosimetry* **89**, 259–262 (2000).

[14] Luís, R. *et al.* Parameter optimization of a planar BEGe detector using Monte Carlo simulations. *Nuclear Instruments and Methods A* **623**, 1014–1019 (2010).

[15] García-Toraño, E., Pozuelo, M. & Salvat, F. Monte Carlo calculations of coincidence-summing corrections for volume sources in gamma-ray spectrometry with Ge detectors. *Nuclear Instruments and Methods A* **544**, 577–583 (2005).

[16] Harkness-Brennan, L. J. *et al.* An experimental characterisation of a Broad Energy Germanium detector. *Nuclear Instruments and Methods A* **760**, 28–39 (2014).

[17] Ješkovský, M., Javorník, A., Breier, R., Slučiak, J. & Povinec, P. P. Experimental and Monte Carlo determination of HPGe detector efficiency. *Journal of Radioanalytical and Nuclear Chemistry* **322**, 1863–1869 (2019).

[18] Ewa, I. O. B., Bodizs, D., Czifrus, S. & Molnar, Z. Monte Carlo determination of full energy peak efficiency for a HPGe detector. *Applied Radiation and Isotopes* **55**, 103–108 (2001).

[19] Deslattes, R. D. *et al.* X-ray transition energies: New approach to a comprehensive evaluation. *Reviews of Modern Physics* **75**, 35–99 (2003).

[20] Scofield, J. H. Relativistic Hartree–Slater values for K and L X-ray emission rates. *Atomic Data and Nuclear Data Tables* **14**, 121–137 (1974).